# Use of Sodium Diethyldithiocarbamate to Enhance the Open-Circuit Voltage of $CH_3NH_3PbI_3$ Perovskite Solar Cells

*Miriam Más-Montoya,* David Curiel, Junke Wang, Bardo J. Bruijnaers, and René A. J. Janssen**

**The incorporation of additives to modulate the properties of metal halide perovskite thin films has become a successful approach in improving the power conversion efficiency of perovskite-based solar cells. Herein, the beneficial use of sodium diethyldithiocarbamate (NaDEDTC) as processing agent in improving the open-circuit voltage of methylammonium lead triiodide perovskite solar cells is reported. DEDTC reduces the rate of perovskite crystallization. Absorption and emission spectra show that the optical bandgap of the perovskite films remain essentially unchanged and X-ray diffraction reveals the formation of preferentially oriented crystallites independent of the use of DEDTC. The use of DEDTC, however, results in a decrease in nonradiative decay as inferred from a two order of magnitude increase in electroluminescence efficiency, explaining the increased open-circuit voltage. Fourier-transform infrared spectroscopy, nuclear magnetic resonance, and X-ray photoelectron spectroscopy show that the DEDTC ligand is not present after the film processing. Therefore, DEDTC modulates film formation but is not incorporated in the perovskite or present as a surface ligand. Sodium ions, on the contrary, are incorporated in the perovskite layer.**

## 1. Introduction

The discovery of lead halide perovskite light-harvesting materials[1] has triggered a thriving development of a new photovoltaic technology in just a decade.[2] Essentially, the success of these hybrid organic–inorganic photoactive materials relies on the outstanding optoelectronic and semiconducting characteristics of these materials and the tunability of these properties by changing the metal, halide, or (in)organic counter ion.[3] The remarkable progress in the performance of perovskite solar cells has led to a certified power conversion efficiency (PCE) of 25.5%.[4] Still many aspects such as those related to the device engineering,[5] material processing methods,[6] interfacial materials design,[7] or compositional variations[8] attract the attention of researchers today. Obtaining a deeper knowledge on the different morphological, optical, and electronic features of these materials is critical to further optimize the photovoltaic technology based on perovskites.

In this regard, the use of additives has become an interesting approach to improve the perovskite properties and the solar cell performance.[9] It has been reported that these components favorably affect the perovskite crystallization kinetics by reducing the reaction rate between the lead salts and the organic precursors, improving the resulting perovskite morphology, passivating the film defects, adjusting the optoelectronic properties, and/or reducing the undesired recombination pathways, among others.[10] The extensive diversity of evaluated additives includes organic[11] and inorganic salts,[12] polymers,[13] small molecules,[14] inorganic acids,[15] or organic solvents.[16]

In general, a common structural feature of the additives is the presence of heteroatoms having lone electron pairs such as N, O, and/or S. These atoms can establish two different types of interaction with the perovskite components. They can interact with the cationic $CH_3NH_3^+$ species via formation of hydrogen bonds. Alternatively, they can participate as Lewis base to form coordinate covalent bonds with the Lewis acid $Pb^{2+}$ atoms of the perovskite. Within the sulfur containing ligands, dithiocarbamates have been widely explored in coordination chemistry.[17] This is mainly due to their easy synthetic accessibility and their ability

Dr. M. Más-Montoya, Dr. D. Curiel
Multifunctional Molecular Materials
Department of Organic Chemistry
Faculty of Chemistry
University of Murcia
Campus of Espinardo, Murcia 30100, Spain
E-mail: miriammas@um.es

Dr. J. Wang, Dr. B. J. Bruijnaers, Prof. R. A. J. Janssen
Molecular Materials and Nanosystems
Institute for Complex Molecular Systems
Eindhoven University of Technology
P.O. Box 513, Eindhoven 5600 MB, The Netherlands
E-mail: r.a.j.janssen@tue.nl

Prof. R. A. J. Janssen
Dutch Institute for Fundamental Energy Research
De Zaale 20, Eindhoven 5612 AJ, The Netherlands

The ORCID identification number(s) for the author(s) of this article can be found under https://doi.org/10.1002/solr.202000811.



**DOI: 10.1002/solr.202000811**

to act as monodentate or bidentate (either as chelating or as bridging) ligands with transition metals, lanthanide, actinide, and main group elements.[18] The properties of dithiocarbamate coordination complexes have permitted their application in the fields of biomedicine,[19] agriculture,[20] and material science,[21] to mention but a few.

Recently, it was reported that by using lead diethyldithiocarbamate in the perovskite precursor mixture the efficiency and stability of inorganic $CsPbI_2Br$ perovskite solar cells were enhanced.[22] The effect was attributed to the fact that lead (II) ions in the perovskite are susceptible to chelating interactions with dithiocarbamate ligands. Here, we investigate the effect of a dithiocarbamate (sodium *N,N*-diethyldithiocarbamate, NaDEDTC) added to a perovskite precursor mixture in different concentrations (5–20 mol%) for organic methylammonium lead triiodide ($CH_3NH_3PbI_3$) solar cells. We find an improved open-circuit voltage ($V_{OC}$) in solar cells processed with the dithiocarbamate additive in comparison with the devices fabricated without. The origin of this improvement has been studied by analyzing the film formation, morphology, electronic properties, and the composition of the perovskite layer. Surprisingly, we find that DEDTC is not present in the resulting $CH_3NH_3PbI_3$ perovskite films and thus modulates film formation but is not acting as surface ligand. Instead, sodium ions are incorporated in the perovskite.

## 2. Results and Discussion

Sodium *N,N*-diethyldithiocarbamate (NaDEDTC) has been explored as additive in processing of methylammonium lead triiodide perovskite-based semiconductor films. The presence of DEDTC ligands and lead (II) cations makes a complexation equilibrium plausible in which the coordination complex $Pb(DEDTC)_2$ forms under the experimental conditions used for the preparation of the perovskite (**Scheme 1**).

For film preparation, we used a hot-casting one-step procedure (**Figure 1**a), dissolving the perovskite precursors ($PbCl_2$ (0.2 M), $Pb(CH_3COO)_2$ (0.8 M), and $CH_3NH_3I$ (3 M)) in *N,N*-dimethylformamide (DMF),[23] together with sodium *N,N*-diethyldithiocarbamate (5, 10, 15, or 20 mol% based on Pb) and warming this solution to 70 °C before spin coating. After spin coating on preconditioned substrates, the layers were annealed at 100 °C to complete the conversion to the perovskite phase. Further details can be found in the Supporting Information. The formation of the $Pb(DEDTC)_2$ coordination complex in the precursors solution can reduce the rate of perovskite formation by complexing and releasing the Pb(II) participating in the equilibrium. This can contribute to tuning the perovskite properties which affect the photovoltaic performance of the devices.

The kinetics of the perovskite formation was highly dependent on the DEDTC content as revealed by the visual appearance of the films right after finishing the spin-coating step (Figure 1b).

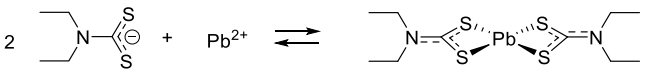


**Scheme 1.** Coordination complex formed between *N,N*-diethyldithiocarbamate and lead (II).

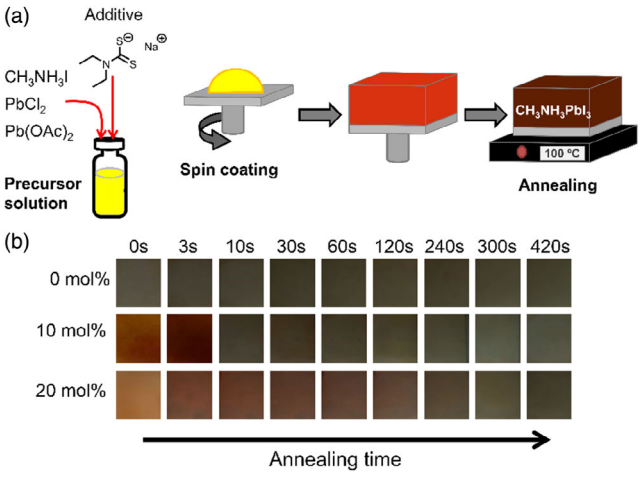


**Figure 1.** a) Schematic representation of the experimental fabrication procedure. b) Evolution of the perovskite film formation with the annealing time at 100 °C upon increasing the ligand concentration. The evolution for the first 7 min is shown.

Thus, in the absence of the ligand the perovskite film was readily formed even prior to thermal annealing, as evidenced by the dark brown color observed in the film. In contrast, when the DEDTC ligand was present the color of the as-deposited film was lighter and the perovskite film required longer annealing times to be formed. This observation proves that the addition of DEDTC restrains the perovskite crystallization as anticipated by the complexation mechanism. In any case, it is worth highlighting that all the perovskites are completely formed after the first 6–7 min of thermal annealing.

As expected, the different rate for the conversion of the precursor solution into the perovskite solid phase is also reflected in the macroscopic morphology of the films. Perovskite films were cast on PEDOT:PSS-coated glass substrates to reproduce the same surface conditions that are used in the fabrication of the photovoltaic devices. Topographic scanning electron microscopy (SEM) images (**Figure 2**) revealed that the larger the amount of DEDTC used (at least up to 15 mol%), the smaller the size of the grains. A similar reduction in grain size was also seen when using DEDTC in the processing of $CsPbI_2Br$ perovskite films.[22] In each case, compact and uniform films with a good surface coverage were obtained, independent of the DEDTC concentration. The fact that we observed a slower color change from yellow to black when using DEDTC (Figure 1b) suggests that the formation of perovskite crystals is retarded. During thermal annealing, the as-formed nuclei (with more DEDTC) have lesser tendency to merge with each other, which reduces the grain size. When the amount of DEDTC exceeded 15 mol%, the characteristic granular-like morphology of the perovskite was lost. In addition, some particles were observed on the film surface most likely due to the accumulation of residual additive. As will be shown, the morphological dissimilarities due to the reduction of the perovskite crystalline grains do not become critical to the solar cell performance. The films consist of densely compacted grains and lead to high efficiencies. Some other reports have also demonstrated that grain boundaries are not detrimental for the device functioning.[24]

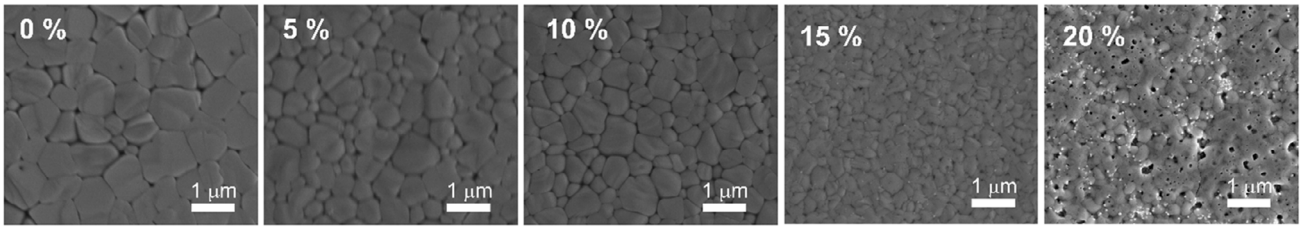


**Figure 2.** Top-view SEM images of the perovskite films processed with different DEDTC percentages.

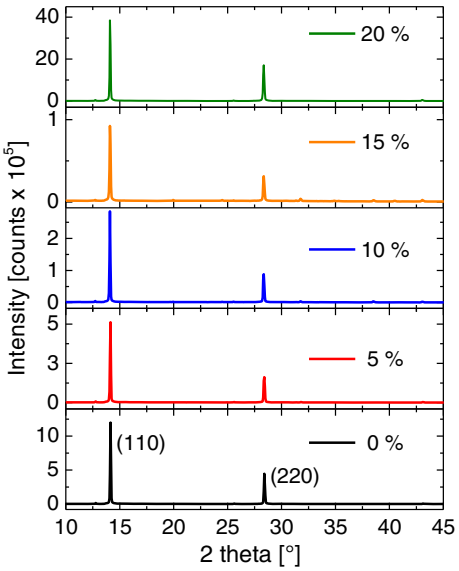


**Figure 3.** XRD patterns of $CH_3NH_3PbI_3$ films, processed with different amounts of DEDTC on glass/PEDOT:PSS substrates.

The identity of the perovskite crystalline structure was investigated by X-ray diffraction (XRD) (**Figure 3**) of the films on glass substrates covered with poly(3,4-ethylenedioxythiophene) polystyrene sulfonate (PEDOT:PSS). The XRD patterns exhibit a preferential orientation because one set of lattice planes is primarily observed. The diffraction peaks located at $2\theta$ values of 14.1° and 28.4° are indexed to the (110) and (220) lattice planes and confirm the crystallinity of the perovskite films. In addition, the analysis of the full width at half maxima (FWHM) determined by fitting the first-order diffraction peak to a Gaussian function revealed a minor widening of the FWHM when going from the pristine perovskite (FWHM = 0.093) to the 15 mol% film (FWHM = 0.117). This fact is in agreement with the smaller grain sizes observed in the SEM images (Figure 2). The reproducibility of the $2\theta$ angles in the compared diffractograms evidences that the same crystalline phase is present in the sequence of films and the addition of DEDTC does not alter the perovskite crystalline structure.

The influence of the addition of DEDTC on the optical properties of the perovskite layers was evaluated by absorption spectroscopy (**Figure 4**a). The position of the optical bandgap ($E_g$) determined from a Tauc plot,[25] remained virtually unchanged with values of 1.60–1.62 eV, consistent with those reported in the literature for $CH_3NH_3PbI_3$ perovskites.[8a] Figure 4b shows that the intensity of the steady-state photoluminescence (PL) of $CH_3NH_3PbI_3$ deposited on PEDOT:PSS is affected by the concentration of DEDTC. The observed trend in the evolution of the PL intensity is correlated with the efficiency of PL quenching via charge transfer from the perovskite layer to the PEDOT:PSS film. The higher PL intensity for the film prepared with 20 mol% DEDTC is tentatively explained by the fact that, in agreement with the previously observed morphology, some perovskite crystallites in these films are poorly connected to the PEDOT:PSS layer.[23] Because the PL intensity is determined by the intrinsic PL quantum yield and by the effectiveness of quenching by the PEDOT:PSS layer, it is useful to compare with the PL intensity on a nonquenching layer. For this purpose we deposited the perovskite layers on polystyrenesulfonic acid (PSSH).[26] As PEDOT:PSS has 1:6 ratio by weight, PSSH preserves much of the surface characteristics of the PEDOT:PSS film. The PL spectra on PSSH are shown in Figure 4c and reveal that the use of 5% or 10% DEDTC increases the PL intensity. A 600-fold enhancement in the PL intensity was observed for the perovskite layer fabricated with 5% DEDTC on PSSH compared with the layer on PSSH without DEDTC. A noticeable PL increase was also detected for the films prepared with 10 mol%, 15 mol%, and no DEDTC, but the PL intensity changed less than a factor 10 for the perovskite layer processed with 20 mol% DEDTC. These results suggest that the efficiency of charge transfer between the perovskite active layer and the PEDOT:PSS layer is improved by the addition of 5–10 mol% of DEDTC.

To explore the effect of the use of DEDTC on the photovoltaic properties, devices with a glass/ITO/PEDOT:PSS/$CH_3NH_3PbI_3$/[60]PCBM/LiF/Al architecture were fabricated (here ITO is indium tin oxide and [60]PCBM phenyl-$C_{61}$-butyric acid methyl ester). Different concentrations of DEDTC (0–20 mol%) were added during the preparation of the photoactive layers. The corresponding photovoltaic parameters are shown in **Table 1** and the current density versus voltage ($J$—$V$) characteristics recorded under simulated sunlight illumination (AM1.5 G, 100 mW cm$^{-2}$) are shown in **Figure 5**a. The control device fabricated without DEDTC achieved a short-circuit current density ($J_{SC}$) of 18.3 mA cm$^{-2}$, an open-circuit voltage ($V_{OC}$) of 0.98 V, and a fill factor (FF) of 0.80, resulting in a maximum PCE of 14.3%. When using DEDTC, a small increase in photocurrent was found (Figure S1, Supporting Information). The $J_{SC}^{EQE}$ obtained by integrating the external quantum efficiency (EQE) spectra (Figure 5b) matches reasonably well with the $J_{SC}$ obtained from the $J$—$V$ curves. One reason for differences between $J_{SC}$ and $J_{SC}^{EQE}$ is seen in the EQE spectra (Figure 5b) where the 5 and 10 mol% samples show an increased EQE above

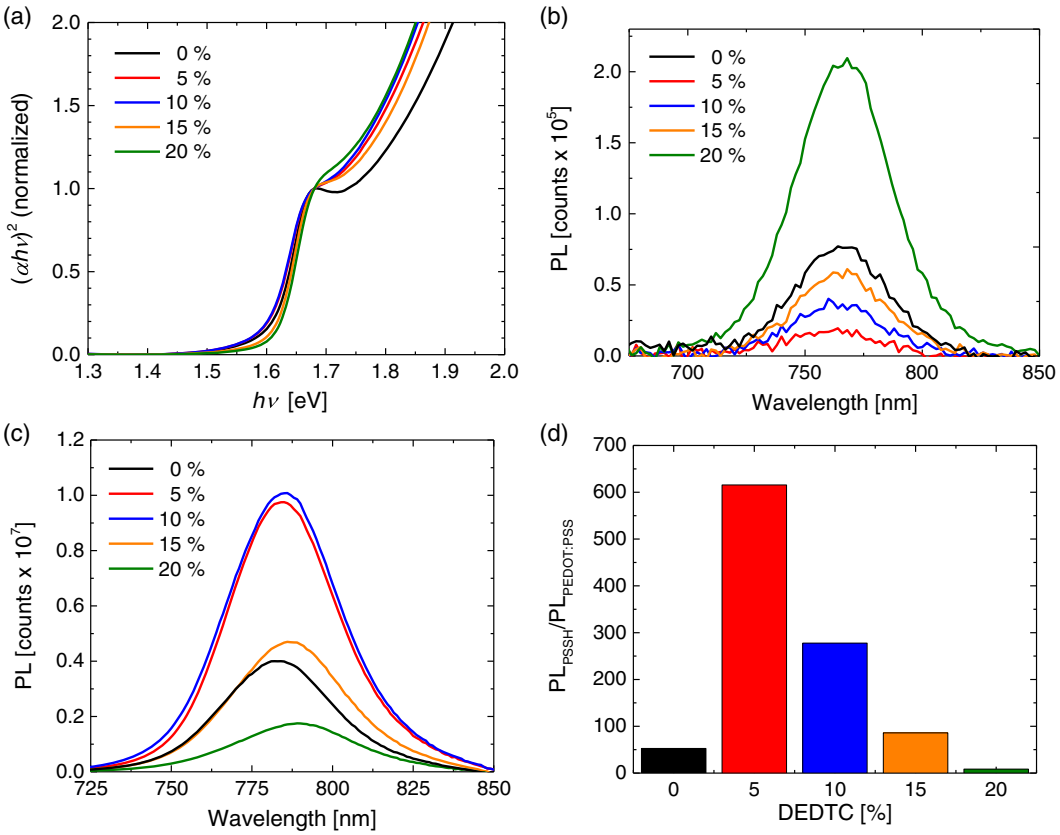


**Figure 4.** Optical characteristics of $CH_3NH_3PbI_3$ films processed with different amounts of DEDTC. a) Normalized Tauc plots. b) PL spectra of $CH_3NH_3PbI_3$ on PEDOT:PSS. c) PL spectra of $CH_3NH_3PbI_3$ on PSSH. d) Ratio of fluorescence intensities at $\lambda_{max}$ for $CH_3NH_3PbI_3$ layers on PSSH relative to layers on PEDOT:PSS.

**Table 1.** Photovoltaic parameters.

| DEDTC [mol%] | $d^{a)}$ [nm] | $J_{SC}$ [mA cm$^{-2}$] | $J_{SC}^{EQEb)}$ [mA cm$^{-2}$] | $V_{OC}$ [V] | FF | PCE [%] | $PCE^{EQEb)}$ [%] |
|---|---|---|---|---|---|---|---|
| 0 | 505 | 18.3 | 18.7 | 0.98 | 0.80 | 14.3 | 14.7 |
| 5 | 560 | 19.3 | 19.0 | 1.01 | 0.75 | 15.5 | 14.4 |
| 10 | 560 | 20.2 | 18.7 | 1.04 | 0.77 | 16.2 | 14.9 |
| 15 | 520 | 18.2 | 16.3 | 1.08 | 0.81 | 15.8 | 14.2 |
| 20 | 600 | 17.1 | 15.4 | 1.05 | 0.82 | 14.7 | 13.3 |

[a)]Film thickness; [b)]$J_{SC}^{EQE}$ calculated by integration of the spectral response with the AM1.5 G spectrum.

630 nm, but lower values between 430 and 630 nm. With the spectral radiance of the solar simulator having relatively more intensity in the red compared with AM1.5 G, such differences can occur. More relevant is the beneficial effect of DEDTC on the $V_{OC}$, which evolves from 0.98 V for the control device up to a maximum value of 1.08 V when 15 mol% of DEDTC was used. The reproducibility of this improvement over a larger number of devices is shown in the statistical distribution represented in Figure 5c and Figure S1 (Supporting Information). The DEDTC ligand has a negligible effect on the hysteresis of the *J*—*V* curves (Figure S2, Supporting Information).

To characterize and identify the recombination mechanisms, dark ($n_d$) and light ($n_l$) ideality factors were determined (**Figure 6**). Typically, an ideality factor of 1 is associated with direct band-to-band or surface recombination, while a value of 2 indicates prevalent trap-assisted Shockley–Read–Hall (SRH) recombination.[27] Differential dark ideality factors were determined from the exponential region of the dark *J*—*V* curves by plotting $n_d$ as defined in Equation (1) versus the applied voltage plot (Figure 6a).[27]

$$n_d = [(k_B T/q)(d\ln J/dV)]^{-1} \quad (1)$$

In Equation (1), $k_B$ is the Boltzmann constant, $T$ is the absolute temperature, and $q$ is the elementary charge. The curves of $n_d$ versus bias voltage show a relatively sharp minimum in the

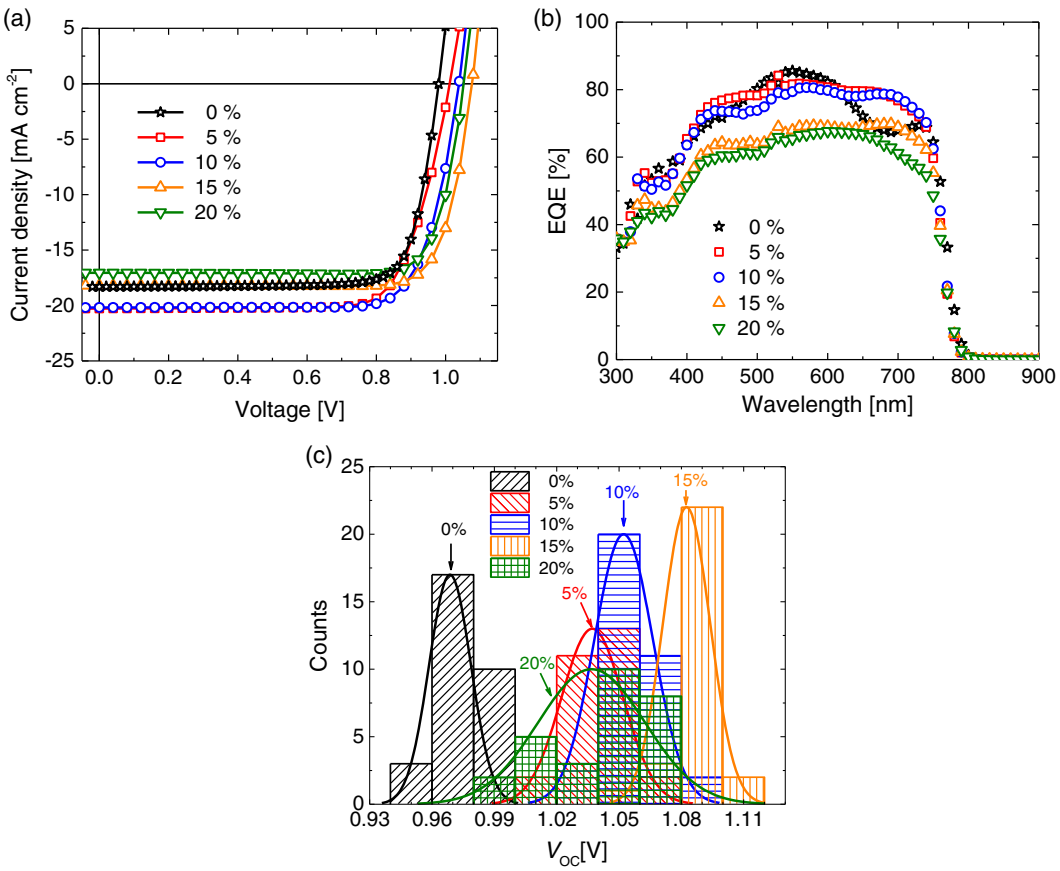


**Figure 5.** Effect of DEDTC on the performance of $CH_3NH_3PbI_3$ solar cells. a) Stabilized *J*—*V* characteristics of the best performing solar cells. b) Corresponding EQE spectra. c) Statistical distribution of the open-circuit voltage ($V_{OC}$).

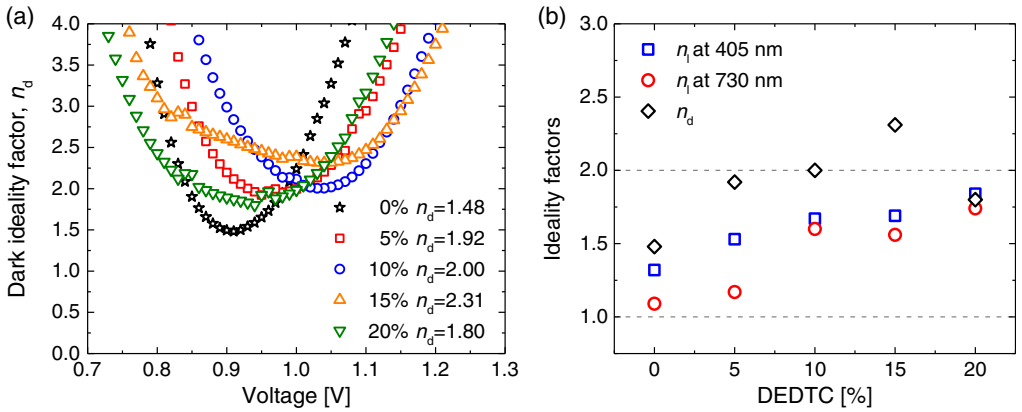


**Figure 6.** a) Dark ideality factors ($n_d$) from the dark *J*–*V* curve as a function of the applied voltage. b) Evolution of dark ($n_d$) and light ($n_l$) ideality factors with the DEDTC percentage.

exponential region of the diode curve (Figure 6a). The increase toward higher and lower voltages is due to the effect of series and shunt resistances and makes that the obtained values for $n_d$ are an upper limit for the real value.[27] A $n_d = 1.48$ was found for the control device ($V_{OC} = 0.98$ V), while $n_d = 2.31$ was obtained for the solar cell based on a 15 mol% of DEDTC ($V_{OC} = 1.08$ V).

Light ideality factors ($n_l$) were determined from the dependence of the $V_{OC}$ on the light intensity expressed as photon flux ($\Phi$) using the expression

$$n_l = \frac{q}{k_B T}\left(dV_{OC}/d\ln\left(\frac{\Phi_0}{\Phi}\right)\right) \quad (2)$$

Figure S3 (Supporting Information) shows the semilogarithmic plots of $V_{OC}$ versus light intensity for illumination at 405 and 730 nm and the resulting $n_l$ values are collected in Figure 6b. As expected, $n_l$ values are lower than $n_d$.[27,28] The ideality factors increase with the increasing amount of DEDTC. The two different wavelengths (405 and 730 nm) used allow to differentiate between recombination processes that occur more toward the front of the device (i.e., near the interface of the hole transporting layer and the perovskite) for UV light while the near-infrared light samples more of the bulk of the photoactive layer.[29] In general, similar ideality factor values were obtained for illumination with both wavelengths (Figure 6b), though blue $n_l$ are slightly higher than red $n_l$. At the same photon flux, the $V_{OC}$'s for 405 and 730 nm illumination were virtually identical for each device (Figure S3, Supporting Information). The fact that both $V_{OC}$ and $n_l$ increase with the increasing percentage of DEDTC suggests less surface recombination when using DEDTC.[30]

The contribution of the nonradiative recombination to the reduction of the open-circuit voltage values with respect to the maximum in the radiative limit was also analyzed by registering the electroluminescence (EL) spectra and the EQE of EL ($EQE_{EL}$). The EL spectra shown in **Figure 7**a reveal no variation in the position of the band maxima and the wavelength is consistent with the PL spectra (Figure 4c). This suggests that the same states are involved in the recombination of both the photogenerated and the electrogenerated electrons and holes. The band shape remains unaffected with the applied voltage (Figure S4, Supporting Information). The $EQE_{EL}$ (Figure 7b) increased with the amount of DEDTC used until reaching a maximum value for 15 mol%. The $EQE_{EL}$ using 10 and 15 mol% of DEDTC is two orders of magnitude higher than that of the control device at an injection current that equals the $J_{SC}$ (**Table 2**). This increased $EQE_{EL}$ signifies reduced nonradiative losses ($\Delta V_{OC,nr}$) and can be correlated to the $V_{OC}$ following expression[31]

$$V_{OC} = \frac{E_g}{q} - \Delta V_{OC,rad} - \Delta V_{OC,nr} = V_{OC,rad} - \frac{k_B T}{q} \ln \frac{1}{EQE_{EL}} \quad (3)$$

A value of 1.31 V was assumed for the radiative limit of the open-circuit voltage ($V_{OC,rad}$) of a $CH_3NH_3PbI_3$-based device.[32] Table 2 shows the different terms of Equation (3) and shows that the calculated $V_{OC}$'s follow the trends in experimental values from $J$—$V$ measurements well. The experiments evidence that the electroluminescent properties of the devices were improved by the addition of DEDTC up to a 15 mol% which reduced the nonradiative recombination ($\Delta V_{OC,nr}$) within the device and improved the achieved $V_{OC}$.

**Table 2.** Experimental and calculated $V_{OC}$.

| DEDTC [mol%] | $V_{OC}$[a)] [V] | $EQE_{EL}$[b)] | $\Delta V_{OC,nr}$[c)] [V] | $V_{OC,\ calc}$[c)] [V] |
|---|---|---|---|---|
| 0 | 0.98 | $1.7 \times 10^{-7}$ | 0.40 | 0.91 |
| 5 | 1.01 | $5.0 \times 10^{-6}$ | 0.31 | 1.00 |
| 10 | 1.04 | $3.4 \times 10^{-5}$ | 0.26 | 1.05 |
| 15 | 1.08 | $6.5 \times 10^{-5}$ | 0.25 | 1.06 |
| 20 | 1.05 | $1.7 \times 10^{-5}$ | 0.28 | 1.03 |

[a)]Extracted from the $J$—$V$ curves; [b)]$EQE_{EL}$ value for an injection current equal to short-circuit current; [c)]Determined using Equation (3).

To analyze the dynamics of the charge recombination processes on the perovskite films, time-resolved PL experiments were performed using the time-correlated single photon counting (TCSPC) technique. The transient PL decays (Figure S5, Supporting Information) fitted better to a biexponential decay function. Slower PL decays were found as the ratio of ligand increased. The longer average PL lifetimes (Table S1, Supporting Information) suggest that the charges can subsist for longer periods within the perovskite films without recombining. This fact could imply a reduced amount of undesired defects, trap states, and/or recombination centers[33] probably passivated by the sodium cations. This observation is in agreement with the reduced nonradiative recombination suggested by the EL experiments, the decreased surface recombination assessed by the light intensity dependent studies, and the improvement of the $V_{OC}$ values due to the use of DEDTC.

Fourier-transform infrared (FTIR) spectroscopy was used to characterize the $CH_3NH_3PbI_3$ perovskite layers fabricated with and without DEDTC and to get a better understanding of the participation of DEDTC in the film processing. **Figure 8** shows the FTIR spectra of NaDEDTC, $Pb(DEDTC)_2$, and those of the perovskite layers fabricated without NaDEDTC and with 20 mol% NaDEDTC, in the latter case before and after performing the

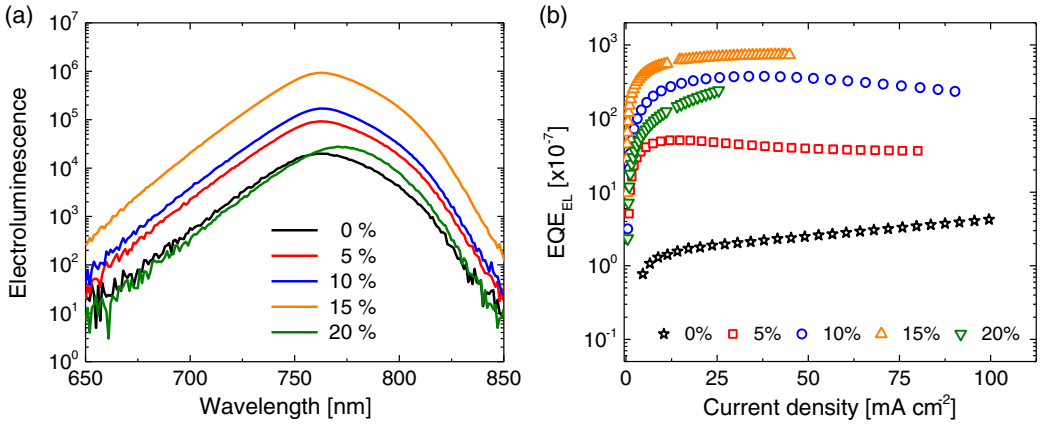


**Figure 7.** a) EL spectra recorded by applying a constant forward voltage of 1.3 V. b) $EQE_{EL}$ as a function of the injected current density.

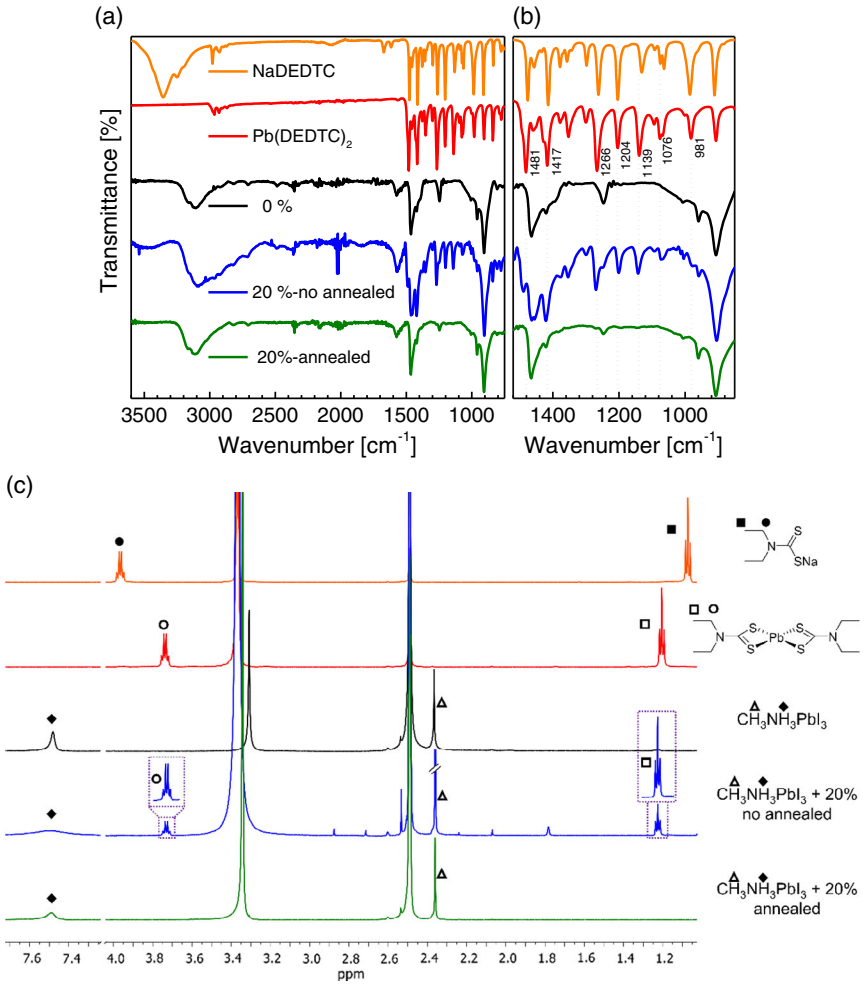


**Figure 8.** FTIR spectra of NaDEDTC, $Pb(DEDTC)_2$, and $CH_3NH_3PbI_3$ layers processed with 0, and 20 mol% DEDTC before and after the annealing. a) Full spectrum. b) Zoom in of the low-energy region. Vertical dashed lines correspond to the frequencies of the characteristic vibrations of $Pb(DEDTC)_2$. c) $^1$H-NMR spectra in DMSO-$d_6$.

thermal treatment of the film. The most representative band of NaDEDTC corresponds to the C—S stretching at 985 $cm^{-1}$. In addition, some other characteristic bands such as N—$CS_2$ stretching (≈1480 $cm^{-1}$) or $R_3C$—N stretching (≈1265 $cm^{-1}$) become useful, along with other very informative bands ascribed to C—H bending and C—C stretching (≈1415, ≈1205, ≈1135, and ≈1070 $cm^{-1}$).[17,18,34] Only marginal differences were observed between the IR wavenumbers of the NaDEDTC and the $Pb(DEDTC)_2$. In addition, the IR spectra acquired with the scratched films of the plain perovskite and the perovskite film prepared with 20 mol % DEDTC (before and after annealing) have been included in this comparison. It is worth highlighting how the IR bands of the perovskite are unequivocally detected in the three compared films. Peaks located at 3166 and 3107 $cm^{-1}$ are ascribed to the N—H stretching vibrations.[35] N—H bending vibrations can be discerned at 1575 and 1465 $cm^{-1}$, while the C—H bending modes are found at 1420 and 1385 $cm^{-1}$. At lower frequencies, the peaks corresponding to the C—H rocking (1247 and 906 $cm^{-1}$) and C—N stretching (959 $cm^{-1}$) are also identified. The conclusive result comes from the clear detection of the dithiocarbamate bands in the film with 20 mol% DEDTC before annealing and how these bands disappear after the thermal treatment to obtain a spectrum identical to that of the pristine perovskite. This sequence of experiments demonstrates that the dithiocarbamate ligand transiently intervenes during the processing of the perovskite film.

To further investigate the evolution of the DEDTC complex in the perovskite films, an additional comparison, analogous to that described by IR spectroscopy, was performed using nuclear magnetic resonance (NMR) experiments (Figure 8c and Figure S6, Supporting Information). In this case, it is worth highlighting how the $^1$H-NMR spectra allow the differentiation between $Na(DEDTC)_2$ and $Pb(DEDTC)_2$ complexes. Both show a triplet at lower chemical shift, ascribed to the $CH_3$, and a more deshielded quartet corresponding to the $CH_2$ group. However, the $Pb(DEDTC)_2$ complex shows the triplet displaced to higher chemical shift ($\delta = 1.21$ ppm) and the quartet displaced to lower chemical shift ($\delta = 3.74$ ppm) when compared with the sodium complex. Concerning the $^1$H-NMR spectra acquired for the scratched film of the plain perovskite ($CH_3NH_3PbI_3$), it shows

two singlets located at $\delta = 7.48$ ppm and at $\delta = 2.36$ ppm attributed to the resonances of the $NH_3^+$ and $CH_3$ of the methylammonium, respectively. These peaks also are perfectly reproduced in the spectra of the films with 20 mol% of DEDTC before and after annealing. At this point, it is important to note that a triplet ($\delta = 1.23$ ppm) and a quartet ($\delta = 3.73$ ppm) peaks are observed in the film without thermal treatment. These confirm the presence of DEDTC ligand (from the starting sodium complex) coordinating the Pb(II) cation. More importantly, the DEDTC signals are lost upon annealing the thin film to obtain a spectrum identical to that of the plain perovskite. These results are corroborated by the $^{13}$C-NMR spectra (Figure S6, Supporting Information) and prove, as previously discussed, the transitory participation of the DEDTC on the perovskite formation.

The thermal transformation of the DEDTC ligand can be related to the known decomposition of dithiocarbamates under acidic conditions, through a dithiodecarboxylation mechanism producing diethylamine and $CS_2$.[36] The much higher p$K_a$ of $CH_3NH_3^+$ compared with HDEDTC indicates that the acid-base equilibrium depicted in **Scheme 2** is shifted toward the side of $DEDTC^-$ and $CH_3NH_3^+$.[37] We hypothesize that the loss of $CS_2$ and other volatile products at the increased temperatures used in the fabrication method provide the driving force for the decomposition of DEDTC. This, along with the lability of DEDTC ligand, gives a possible explanation for the absence of that ligand in the processed perovskite layers. In addition, the diethylamine formed can protonate because the p$K_a$ of its associated acid is similar to that of $CH_3NH_3^+$.[36] The methylamine (boiling point [b.p.] = −6.3 °C) formed in this reaction evaporates more readily than diethylamine (b.p. = 55 °C) during processing and thermal annealing. The remaining sodium cation will compensate the charge balance with the iodide anion present in the reaction mixture.

X-ray photoelectron spectroscopy (XPS) experiments were performed to compare the composition of pristine perovskite films with those fabricated with DEDTC (Figure S7, Supporting Information), both at the surface and in the bulk. Carbon (C), nitrogen (N), lead (Pb), sodium (Na), and sulfur (S) atoms were probed. The expected signals for C 1s at 286.3 eV and N 1s at 402.8 eV of $CH_3NH_3^+$ were observed.[38] The most noticeable feature observed in the XPS spectra with increasing concentration of DEDTC in the processing was the emergence of a shoulder at lower binding energies (284 and 400 eV) than C 1s and N 1s core-level signals of the perovskite (Figure S7a,b, Supporting Information). The additional signal at 284 eV can be attributed to C—C bonds present in diethylamine formed in the decomposition of DEDTC ligand (Scheme 2). Likewise, the signal at 400 eV may point to the presence of amines, such as methylamine[39] and/or diethylamine. Concerning the evolution of the Pb 4f core-level spectra, the two main peaks ascribed to Pb(II) do not experience any significant change. The weaker peaks assigned to the Pb(0) signals at 141.8 and 136.9 eV reduced their intensity and disappeared as the DEDTC concentration increases (Figure S7c, Supporting Information). These results show that the presence of DEDTC ligand during the perovskite processing has a detectable effect on the resulting active layer. Additional information is obtained from the S 2p and Na 1s signals. These elements can only originate from NaDEDTC as processing agent and, as expected, no Na 1s and S 2p signals are detected in the control XPS experiments on pristine perovskite layers. However, also no S 2p signal is observed for the sample prepared with 10 mol% of DEDTC and only a negligible deviation from the baseline is detected when 20 mol% of DEDTC is used. Conversely, the evolution of the Na 1s peak shows a growing peak when going from 0, via 10, to 20 mol% of NaDEDTC. This result fits with the proposed dithiodecarboxylation of DEDTC, as shown in Scheme 2, whose cleavage while forming diethylamine and volatile $CS_2$ also leaves behind the $Na^+$ ion that can be incorporated in the perovskite. Indeed, alkali atoms, including $Na^+$, have been widely reported to improve perovskite solar cell performance.[40]

XPS-depth profiling experiments (**Figure 9**) confirmed these observations when following the distribution of the different elements across the film thickness (directly correlated to the sputtering time). In general, the atomic concentrations of Pb, C, and N were approximately uniform throughout the film thickness for the different tested samples. As expected, no sodium was detected in the control perovskite sample (Figure 9a,d). Nevertheless, the presence of sodium was clearly manifested for the perovskite layer prepared with 10 and 20 mol% of DEDTC ligand. The distribution of the sodium cation detected across the layers fabricated with 10 or 20 mol% DEDTC concentration was somewhat different (Figure 9d). No sulfur was detected in any of the perovskite samples (Figure S8, Supporting Information). This fact supports our hypothesis that the DEDTC decomposes under the conditions of film formation via the mechanism in Scheme 2, and involves the cleavage of a carbon disulfide molecule, which due to its low boiling point (b.p. = 46 °C), will evaporate.[36b,41] In a scenario where the DEDTC persists in the perovskite films, the S atomic

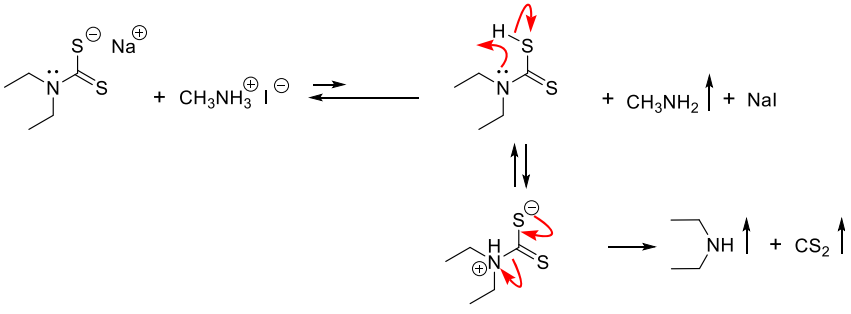


**Scheme 2.** Decomposition of DEDTC under influence of methylammonium.

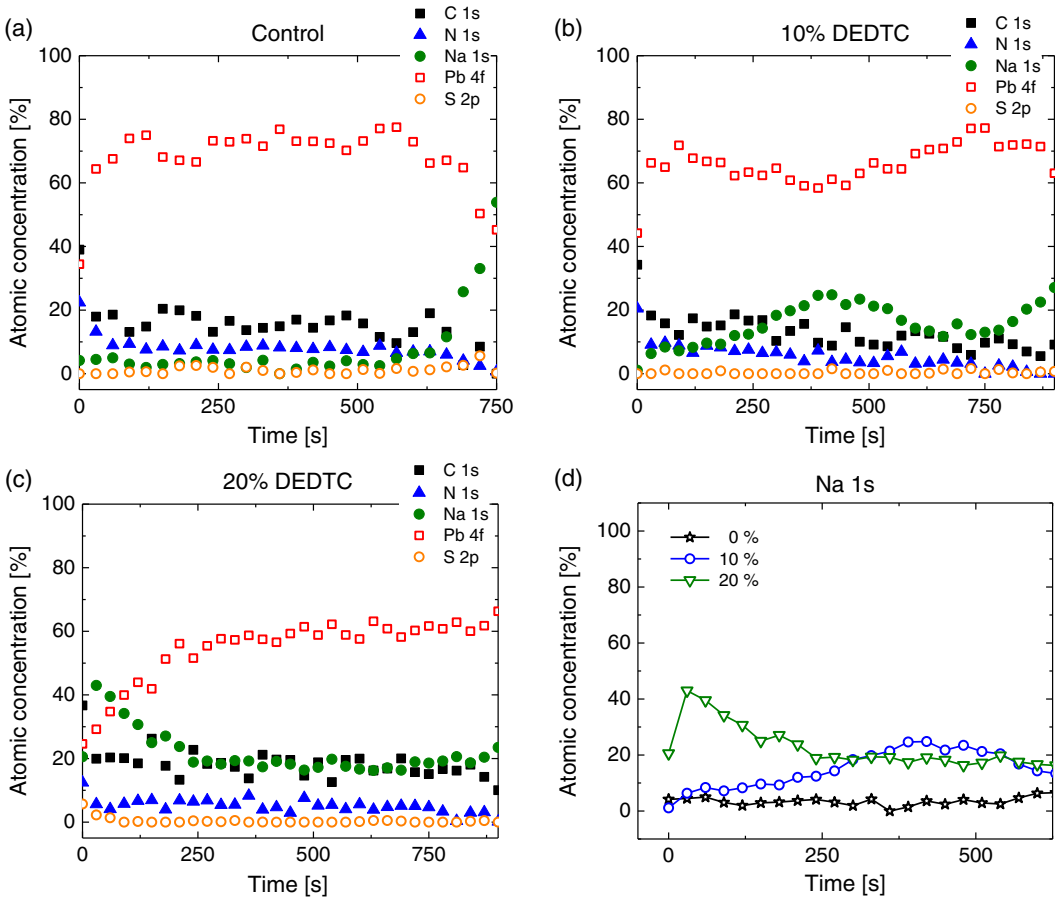


**Figure 9.** XPS-depth profiles of a) the control $CH_3NH_3PbI_3$ film, and $CH_3NH_3PbI_3$ containing b) 10 mol% and c) 20 mol% of DEDTC; d) comparison of the atomic concentration of the core-level spectra of Na 1s at the different amounts of DEDTC analyzed.

concentration would double that of Na. Thus, the sodium ions remaining in the perovskite film could passivate the ionic vacancies and hinder the undesired iodide motion within the perovskite lattice, which might be one of the reasons of the improvement of the device functioning.[42] In agreement with the investigated dithiocarbamate concentrations, a 5–10 mol% does not seem to have a detrimental effect on the formation and performance of the perovskite layer because improved photovoltaic performance is experimentally corroborated.

## 3. Conclusions

In summary, the incorporation of NaDEDTC into the perovskite precursor solution improved the open-circuit voltage of $CH_3NH_3PbI_3$-based devices. In the presence of DEDTC, the formation of the perovskite phase is retarded by coordination of lead ions. The presence of DEDTC did not change the crystalline structure of the perovskite layer, but reduced the grain size. The use of DEDTC resulted in perovskite layers with enhanced photovoltaic performance via an improved charge transfer between the perovskite active layer and the PEDOT:PSS hole transporting layer, and, second, via a reduction of nonradiative recombination as inferred from an increased EL efficiency. The combination of these effects led to a significant improved open-circuit voltage. FTIR, NMR, and XPS studies conducted to investigate the composition of the layers revealed that no DEDTC is present in the perovskite films after processing and we propose that it decomposes during film formation. Evidence was found for an increased concentration of sodium ions in the perovskite films. Although sodium ions are known to passivate defects and vacancies in the perovskite films, it is at present not clear to what extent these participate in improving the device performance. The investigation demonstrates how the use of cleavable additives that can participate in the fabrication of perovskite films via a transient chelating effect offers a useful approach for device processing and may form a starting point for developing novel dithiocarbamate-based ligands that contribute to the progress of hybrid photovoltaics.

## Supporting Information

Supporting Information is available from the Wiley Online Library or from the author.

## Acknowledgements

The authors acknowledge financial support from the Ministry of Science, Innovation and Universities (Project RTI2018-101092-B-I00), and

Programa Estatal de Fomento de la Investigación Científica y Técnica de Excelencia (RED2018-102815-T). The authors also thank Fundación Séneca–Agencia de Ciencia y Tecnología de la Región de Murcia for funding the Project 20959/PI/18 and M.M.-M. postdoctoral contract from "Saavedra Fajardo Program" (20406/SF/17). This research was further funded by the European Research Council under the European Union's Seventh Framework Programme (FP/2007–2013)/ERC Grant Agreement No. 339031 and from the Ministry of Education, Culture and Science (Gravity program 024.001.035).

## Conflict of Interest

The authors declare no conflict of interest.

## Data Availability Statement

Research data are not shared.

## Keywords

additives, dithiocarbamate, perovskite solar cells

Received: December 21, 2020
Revised: February 2, 2021
Published online: February 17, 2021

[1] A. Kojima, K. Teshima, Y. Shirai, T. Miyasaka, *J. Am. Chem. Soc.* **2009**, *131*, 6050.
[2] A. K. Jena, A. Kulkarni, T. Miyasaka, *Chem. Rev.* **2019**, *119*, 3036.
[3] J. Huang, Y. Yuan, Y. Shao, Y. Yan, *Nat. Rev. Mater.* **2017**, *2*, 17042.
[4] National Renewable Energy Laboratory, https://www.nrel.gov/pv/assets/pdfs/best-research-cell-efficiencies.20200311.pdf (accessed: December 2020).
[5] T. Salim, S. Sun, Y. Abe, A. Krishna, A. C. Grimsdale, Y. M. Lam, *J. Mater. Chem. A* **2015**, *3*, 8943.
[6] a) W. A. Dunlap-Shohl, Y. Zhou, N. P. Padture, D. B. Mitzi, *Chem. Rev.* **2019**, *119*, 3193; b) F. Huang, M. Li, P. Siffalovic, G. Cao, J. Tian, *Energy Environ. Sci.* **2019**, *12*, 518.
[7] M. Hadadian, J.-H. Smått, J.-P. Correa-Baena, *Energy Environ. Sci.* **2020**, *13*, 1377.
[8] a) J. H. Noh, S. H. Im, J. H. Heo, T. N. Mandal, S. I. Seok, *Nano Lett.* **2013**, *13*, 1764; b) W. Li, Z. Wang, F. Deschler, S. Gao, R. H. Friend, A. K. Cheetham, *Nat. Rev. Mater.* **2017**, *2*, 16099.
[9] a) T. Li, Y. Pan, Z. Wang, Y. Xia, Y. Chen, W. Huang, *J. Mater. Chem. A* **2017**, *5*, 12602; b) A. Mahapatra, D. Prochowicz, M. M. Tavakoli, S. Trivedi, P. Kumar, P. Yadav, *J. Mater. Chem. A* **2020**, *8*, 27; c) B. Li, D. Binks, G. Cao, J. Tian, *Small* **2019**, *15*, 1903613; d) S. Liu, Y. Guan, Y. Sheng, Y. Hu, Y. Rong, A. Mei, H. Han, *Adv. Energy Mater.* **2019**, 1902492; e) F. Zhang, K. Zhu, *Adv. Energy Mater.* **2019**, 1902579.
[10] H. Zhang, M. K. Nazeeruddin, W. C. H. Choy, *Adv. Mater.* **2019**, *31*, 1805702.
[11] M. E. Kayesh, K. Matsuishi, R. Kaneko, S. Kazaoui, J.-J. Lee, T. Noda, A. Islam, *ACS Energy Lett.* **2019**, *4*, 278.
[12] N. Li, S. Tao, Y. Chen, X. Niu, C. K. Onwudinanti, C. Hu, Z. Qiu, Z. Xu, G. Zheng, L. Wang, Y. Zhang, L. Li, H. Liu, Y. Lun, J. Hong, X. Wang, Y. Liu, H. Xie, Y. Gao, Y. Bai, S. Yang, G. Brocks, Q. Chen, H. Zhou, *Nat. Energy* **2019**, *4*, 408.
[13] T.-H. Han, J.-W. Lee, C. Choi, S. Tan, C. Lee, Y. Zhao, Z. Dai, N. De Marco, S.-J. Lee, S.-H. Bae, Y. Yuan, H. M. Lee, Y. Huang, Y. Yang, *Nat. Commun.* **2019**, *10*, 520.
[14] a) C. Qin, T. Matsushima, T. Fujihara, C. Adachi, *Adv. Mater.* **2017**, *29*, 1603808; b) S. Masi, A. Rizzo, R. Munir, A. Listorti, A. Giuri, C. Esposito Corcione, N. D. Treat, G. Gigli, A. Amassian, N. Stingelin, S. Colella, *Adv. Energy Mater.* **2017**, *7*, 1602600; c) M. Qin, J. Cao, T. Zhang, J. Mai, T.-K. Lau, S. Zhou, Y. Zhou, J. Wang, Y.-J. Hsu, N. Zhao, J. Xu, X. Zhan, X. Lu, *Adv. Energy Mater.* **2018**, *8*, 1703399.
[15] J. H. Heo, D. H. Song, H. J. Han, S. Y. Kim, J. H. Kim, D. Kim, H. W. Shin, T. K. Ahn, C. Wolf, T.-W. Lee, S. H. Im, *Adv. Mater.* **2015**, *27*, 3424.
[16] N. Ahn, D.-Y. Son, I.-H. Jang, S. M. Kang, M. Choi, N.-G. Park, *J. Am. Chem. Soc.* **2015**, *137*, 8696.
[17] a) P. J. Heard, *Prog. Inorg. Chem.*, **2005**, *53*, 1; b) G. Hogarth, *Prog. Inorg. Chem.*, **2005**, *53*, 71.
[18] A. Constantino Fabretti, A. Giusti, C. Preti, G. Tosi, P. Zannini, *Polyhedron* **1986**, *5*, 871.
[19] a) J. W. d. F. Oliveira, H. A. O. Rocha, W. M. T. Q. de Medeiros, M. S. Silva, *Molecules* **2019**, *24*, 2806; b) S. Zdenek, C. Boris, *Med. Chem.* **2012**, *12*, 1184; c) L. Brustolin, C. Nardon, N. Pettenuzzo, N. Zuin Fantoni, S. Quarta, F. Chiara, A. Gambalunga, A. Trevisan, L. Marchiò, P. Pontisso, D. Fregona, *Dalton Trans.* **2018**, *47*, 15477.
[20] a) R. Kesari, V. K. Gupta, *Talanta* **1998**, *45*, 1097; b) G. Vettorazzi, W. F. Almeida, G. J. Burin, R. B. Jaeger, F. R. Puga, A. F. Rahde, F. G. Reyes, S. Schvartsman, *Teratogen. Carcin. Mut.* **1995**, *15*, 313.
[21] a) P. A. Ajibade, B. C. Ejelonu, *Spectrochim. Acta A* **2013**, *113*, 408; b) A. Angeloski, A. R. Gentle, J. A. Scott, M. B. Cortie, J. M. Hook, M. T. Westerhausen, M. Bhadbhade, A. T. Baker, A. M. McDonagh, *Inorg. Chem.* **2018**, *57*, 2132.
[22] J. He, J. Liu, Y. Hou, Y. Wang, S. Yang, H. G. Yang, *Nat. Commun.* **2020**, *11*, 4237.
[23] J. J. van Franeker, K. H. Hendriks, B. J. Bruijnaers, M. W. G. M. Verhoeven, M. M. Wienk, R. A. J. Janssen, *Adv. Energy Mater.* **2017**, *7*, 1601822.
[24] a) W.-J. Yin, T. Shi, Y. Yan, *Adv. Mater.* **2014**, *26*, 4653; b) J. S. Yun, A. Ho-Baillie, S. Huang, S. H. Woo, Y. Heo, J. Seidel, F. Huang, Y.-B. Cheng, M. A. Green, *J. Phys. Chem. Lett.* **2015**, *6*, 875; c) T. S. Sherkar, C. Momblona, L. Gil-Escrig, J. Ávila, M. Sessolo, H. J. Bolink, L. J. A. Koster, *ACS Energy Lett.* **2017**, *2*, 1214.
[25] a) J. Tauc, *Mater. Res. Bull.* **1968**, *3*, 37; b) A. Dolgonos, T. O. Mason, K. R. Poeppelmeier, *J. Solid State Chem.* **2016**, *240*, 43.
[26] K. H. Hendriks, J. J. van Franeker, B. J. Bruijnaers, J. A. Anta, M. M. Wienk, R. A. J. Janssen, *J. Mater. Chem. A* **2017**, *5*, 2346.
[27] W. Tress, M. Yavari, K. Domanski, P. Yadav, B. Niesen, J. P. Correa Baena, A. Hagfeldt, M. Graetzel, *Energy Environ. Sci.* **2018**, *11*, 151.
[28] a) T. Kirchartz, F. Deledalle, P. S. Tuladhar, J. R. Durrant, J. Nelson, *J. Phys. Chem. Lett.* **2013**, *4*, 2371; b) G. A. H. Wetzelaer, M. Kuik, M. Lenes, P. W. M. Blom, *Appl. Phys. Lett.* **2011**, *99*, 153506; c) K. Tvingstedt, C. Deibel, *Adv. Energy Mater.* **2016**, *6*, 1502230.
[29] J.-P. Correa-Baena, W. Tress, K. Domanski, E. H. Anaraki, S.-H. Turren-Cruz, B. Roose, P. P. Boix, M. Grätzel, M. Saliba, A. Abate, A. Hagfeldt, *Energy Environ. Sci.* **2017**, *10*, 1207.
[30] a) B. J. Bruijnaers, E. Schiepers, C. H. L. Weijtens, S. C. J. Meskers, M. M. Wienk, R. A. J. Janssen, *J. Mater. Chem. A* **2018**, *6*, 6882; b) K. Tvingstedt, L. Gil-Escrig, C. Momblona, P. Rieder, D. Kiermasch, M. Sessolo, A. Baumann, H. J. Bolink, V. Dyakonov, *ACS Energy Lett.* **2017**, *2*, 424.
[31] a) S. D. Stranks, *ACS Energy Lett.* **2017**, *2*, 1515; b) W. Tress, N. Marinova, O. Inganäs, M. K. Nazeeruddin, S. M. Zakeeruddin, M. Graetzel, *Adv. Energy Mater.* **2015**, *5*, 1400812.

[32] K. Tvingstedt, O. Malinkiewicz, A. Baumann, C. Deibel, H. J. Snaith, V. Dyakonov, H. J. Bolink, *Sci. Rep.* **2014**, *4*, 6071.
[33] a) V. S. Chirvony, J. P. Martínez-Pastor, *J. Phys. Chem. Lett.* **2018**, *9*, 4955; b) W. S. Yang, B.-W. Park, E. H. Jung, N. J. Jeon, Y. C. Kim, D. U. Lee, S. S. Shin, J. Seo, E. K. Kim, J. H. Noh, S. I. Seok, *Science* **2017**, *356*, 1376; c) X. Li, D. Bi, C. Yi, J.-D. Décoppet, J. Luo, S. M. Zakeeruddin, A. Hagfeldt, M. Grätzel, *Science* **2016**, *353*, 58; d) N. De Marco, H. Zhou, Q. Chen, P. Sun, Z. Liu, L. Meng, E.-P. Yao, Y. Liu, A. Schiffer, Y. Yang, *Nano Lett.* **2016**, *16*, 1009.
[34] H. L. M. Van Gaal, J. W. Diesveld, F. W. Pijpers, J. G. M. Van der Linden, *Inorg. Chem.* **1979**, *18*, 3251.
[35] T. Glaser, C. Müller, M. Sendner, C. Krekeler, O. E. Semonin, T. D. Hull, O. Yaffe, J. S. Owen, W. Kowalsky, A. Pucci, R. Lovrinčić, *J. Phys. Chem. Lett.* **2015**, *6*, 2913.
[36] a) A. E. Martin, *Anal. Chem.* **1953**, *25*, 1260; b) P. R. Heckley, D. G. Holah, A. N. Hughes, F. Leh, *Can. J. Chem.* **1970**, *48*, 3827.
[37] pKa (HDEDTC) = 3.95. It can be assumed that the difference between the pKa values will also remain large in DMF.
[38] a) C. Rocks, V. Svrcek, P. Maguire, D. Mariotti, *J. Mater. Chem. C* **2017**, *5*, 902; b) C. Das, M. Wussler, T. Hellmann, T. Mayer, W. Jaegermann, *Phys. Chem. Chem. Phys.* **2018**, *20*, 17180.
[39] M.-C. Jung, Y. M. Lee, H.-K. Lee, J. Park, S. R. Raga, L. K. Ono, S. Wang, M. R. Leyden, B. D. Yu, S. Hong, Y. Qi, *Appl. Phys. Lett.* **2016**, *108*, 073901.
[40] C. Li, A. Wang, L. Xie, X. Deng, K. Liao, J.-A. Yang, T. Li, F. Hao, *J. Mater. Chem. A* **2019**, *7*, 24150.
[41] a) R. R. Vandebeek, S. J. Joris, K. I. Aspila, C. L. Chakrabarti, *Can. J. Chem.* **1970**, *48*, 2204; b) S. J. Joris, K. I. Aspila, C. L. Chakrabarti, *J. Phys. Chem.* **1970**, *74*, 860.
[42] a) J. Cao, S. X. Tao, P. A. Bobbert, C.-P. Wong, N. Zhao, *Adv. Mater.* **2018**, *30*, 1707350; b) W. Zhao, Z. Yao, F. Yu, D. Yang, S. Liu, *Adv. Sci.* **2018**, *5*, 1700131; c) B. Chen, P. N. Rudd, S. Yang, Y. Yuan, J. Huang, *Chem. Soc. Rev.* **2019**, *48*, 3842.